A Numerical Study on the Formation of Organized Convective Storms: Part I. Formation Patterns of Long-Lasting Cells

By Ryohei Misumi[1], Marjan Divjak[2], Shuichi Tanahashi[3] and Takao Takeda

Institute for Hydrospheric-Atmospheric Sciences, Nagoya University, Chikusa-ku, Nagoya 464-01, Japan

(Manuscript received 21 April 1992, in revised form 2 February 1994)

Abstract

A three-dimensional numerical simulation of a convective-cloud ensemble was performed in order to study the formation process of long-lasting precipitating convective cells. As the initial condition, random small thermals were given in the horizontally homogeneous atmosphere.

The convective cells were classified into three types: The first type (S-type) was short-lived and had a downshear-tilting updraft. The second type (F-type) was forced by the other cells and persisted for a long time, although the airflow structure was similar to S-type. The third type (L-type) was long-lasting and had an upshear-tilting updraft.

In the formation process of an L-type cell, the updraft root must move in a downshear direction faster than the rising air parcels in order to build an upshear-tilting updraft. The fast movement of the updraft root is initially forced by the neighboring cells. The results showed there are three patterns in this process. In Pattern I the updraft root moves with outflow diverging from one short-lived cell. In Pattern II it moves with outflow boundaries of several short-lived cells which form successively. In Pattern III it moves together with outflow diverging from a pre-existing L-type cell. Once an upshear-tilting updraft is built, the cell produces a strong cold air pool near the surface and is self-maintained at its edge.

1. Introduction

Generally, a cumulonimbus cloud consists of several precipitating convective cells. The life-times of the cells are usually a few tens of minutes, but sometimes special cells which persist for more than several hours are observed. Typical of such long-lasting cells is a supercell storm, which consists of one updraft and one downdraft, and persists for several hours (*e.g.*, Browning and Ludlam, 1962; Fankhauser, 1971; Seko and Takeda, 1987). In Japan, long-lasting convective echoes whose horizontal scales are much smaller than supercell storms are sometimes observed (*e.g.*, Takeda and Imai, 1976; Tabata *et al.*, 1989). These cells are also regarded as long-lasting precipitating convective cells.

It is rather rare that such long-lasting cells are completely isolated, and they are usually surrounded by many short-lived cells. For example, Takeda and Imai (1976) observed that a few long-lasting convective echoes appeared among many short-lived echoes. Bluestein and Parker (1993) showed supercell storms often formed among a few ordinary cells. It is very strange that only a few cells can persist for a long time among many other cells, although all the cells exist under a similar atmospheric condition. This variability in the life-time is considered to result from the interaction of convective cells. The main purpose of this study is to discuss the convective-cell interactions which act in the formation process of a long-lasting cell.

Long-lasting cells have common features in their airflow structure. In the case of ordinary cells, the updraft tilts in the direction of the vertical wind shear. The downdraft, which is located to the downshear side, cuts off the supply of warm and moist air into the updraft. In the case of long-lasting cells, however, the updraft tilts against the direction of the vertical wind shear and the downdraft is located on the upshear side (Browning and Ludlam, 1962). This arrangement of airflow is favorable for the maintenance of a convective cell because the downdraft does not cut off the supply of warm

[1]National Research Institute for Earth Science and Disaster Prevention, Tsukuba 305, Japan
[2]Hydrometeorological Institute of Slovenia, Ujubljana
[3]Fujitsu Corporation, Shinkamata 1-17-25, Ohta-Ku, Tokyo 144, Japan

and moist air into the updraft. Earlier investigators questioned why the updraft could tilt against the direction of the vertical wind shear. Takeda (1971) used a two-dimensional numerical model and showed that an upshear-tilting updraft formed when an ambient vertical shear changed its direction at a certain level. Seitter and Kuo (1983) studied the formation of an upshear-tilting updraft in a uni-directinal vertical shear. They concluded that the updraft is tilted by the effect of water loading and evaporative cooling of precipitating water. The results of Fovell and Ogura (1988) more clearly indicate the mechanism of the upshear-tilt: At the leading edge of a cold-air pool, which is produced by evaporative cooling of precipitating water, the hydrostatic pressure gradient is directed to the downshear side in the lower layer. It forces an updraft root to the downshear side and tilts the updraft to the upshear-direction.

The results of these studies made clear the mechanism of upshear-tilting updraft formation. But it is not always clear how the situation in which the mechanism act is produced by convective-cell interactions. In the simulations of long-lasting cells, large isolated thermals, whose horizontal scale is about 20 km, are often given as initial disturbances to simulate upshear-tilting updrafts (*e.g.*, Wilhelmson and Klemp, 1978; Clark, 1979; Schlesinger, 1980). However, such a large thermal does not exist in the real atmosphere. It is considered that some interaction processes play the rôle of such an artificial thermal. The present paper focuses on these processes.

An observational study on convective-cell interactions is very difficult because it needs dense three-dimensional data for various meteorological components. Therefore, the use of a three-dimensional numerical model is reasonable for this study. Three-dimensional numerical simulation of a convective-cloud ensemble has been performed by some modellers. Tao and Soong (1986) evaluated the collective feedback effect of a convective-cloud ensemble on the large-scale atmosphere. Balaji and Clark (1988) simulated the formation process of a cumulonimbus cloud from a cumulus-cloud ensemble. Tao and Simpson (1989a) simulated squall-lines which developed from many small thermals. Tao and Simpson (1989b) also studied the merging process of convective clouds by numerical simulation.

In the present study we perform a three-dimensional numerical simulation of a convective-cloud ensemble. The results of the computations are analyzed by paying special attention as to how convective cells produce a long-lasting cell.

2. The numerical model and initial field

2.1 The model

The following assumptions are adopted in our numerical model.

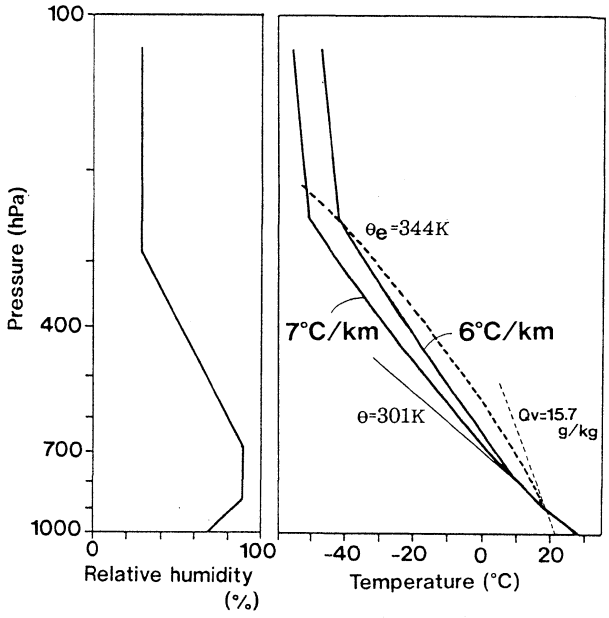

Fig. 1. Initial vertical profiles of temperature and humidity. For reference, 344 K moist adiabat, 15.7 g/kg mixing ratio and 301 K dry adiabat lines are also shown. The thick broken line represents a parcel ascent from the surface based on a surface mixing ratio 15.7 g/kg.

(a) Air motions in the model are anelastic and the Coriolis force is neglected.

(b) The friction and the orographic effect at the lower boundary are neglected.

(c) The absorption and release of latent heat associated with ice-phase processes are not considered.

(d) Condensed-water is divided into cloud water, whose falling velocity relative to the air is negligible, and precipitating water.

(e) Precipitating water evaporates in the absence of cloud water.

The equation of motion, and the prognostic equation for the potential temperature and water substance are similar to those used by Yoshizaki (1978), except for the formation rate of precipitating water. Details of the model description are presented in Appendix A.

The domain for computation has a height of 15 km and a width of 150 km. Mesh sizes are 0.5 km as Δz, and 2 km as Δx and Δy. The variables are arranged in a staggered way similar to Yoshizaki (1978).

It is assumed that the upper and lower boundaries are rigid and that the air slips freely at the boundaries. For potential temperature and water substance, the normal gradients are assumed to be

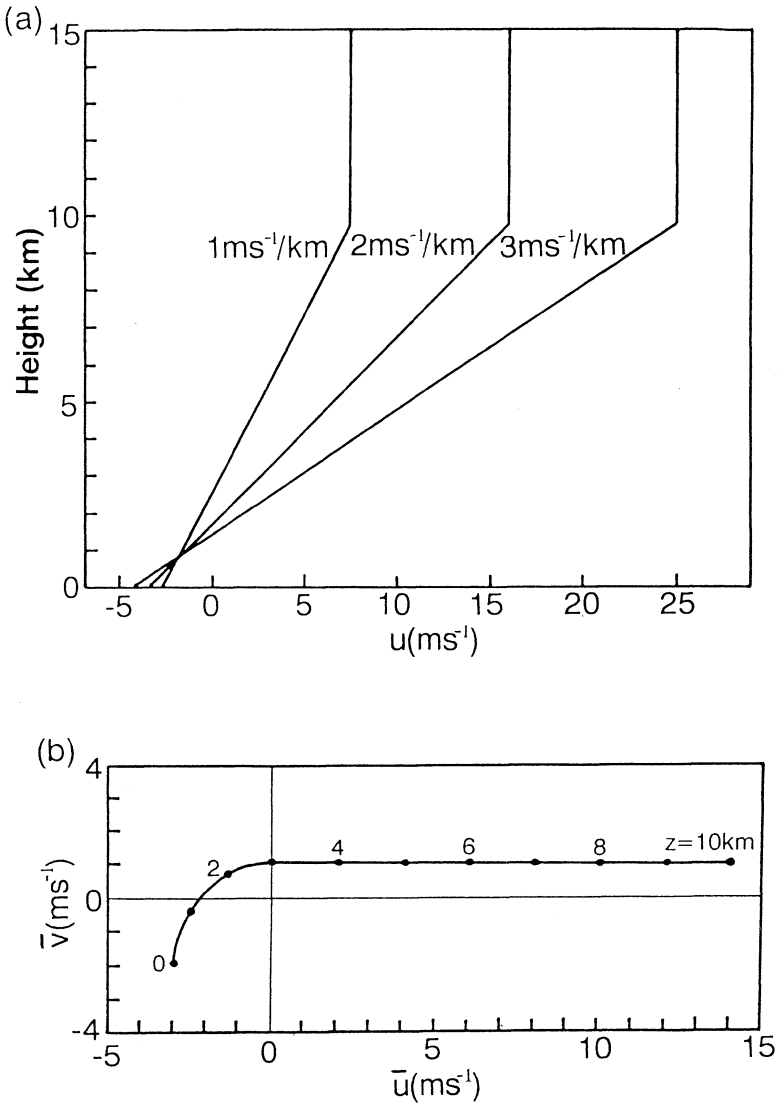

Fig. 2. (a) Vertical profiles of initial ambient wind for uni-directional shear cases. (b) Vertical change in wind direction for a veering wind case.

zero at the lower boundary, and these variables remain undisturbed at the upper boundary. For tangential velocity components, potential temperature and water substance across lateral boundaries, the horizontal gradients are assumed to be zero. For the normal velocity components, the radiation boundary condition (Orlanski,1976) is adopted in order to minimize the reflection of gravity waves at the lateral boundaries.

2.2 Initial field

The vertical profiles of the temperature and relative humidity in the basic field are shown in Fig. 1. The surface temperature is 27.75°C. The lapse rate of the temperature is 9°C/km from the surface to 1.25 km, 8°C/km from 1.25 km to 1.75 km, and 1°C/km from 10.75 km to the top. In the layer from 1.75 km to 10.75 km, two lapse rates of 7°C/km and 6°C/km are given. The CAPE (convective available potential energy) is 3010 m^2/s^2 and 2380 m^2/s^2 in the two lapse rates, respectively. The CAPE of 3010 m^2/s^2 is a rather high value in the real atmosphere. By giving such a large CAPE, it is expected that a lot of convective cells will develop and many interaction patterns will occur in the domain. The effects of the instability of the atmosphere will be discussed by comparing the results of the two lapse rates. CIN (convective inhibition) is 17 m^2/s^2 in both lapse rates. The pressure at the surface is 1000 mb and hydrostatic balance is initially assumed.

Four types of wind fields are initially given. In three types, the initial wind velocity is zero in the y-direction and vertical wind shear is given only in x-direction, as shown in Fig. 2a. In order to examine whether the process found in a unidirectional

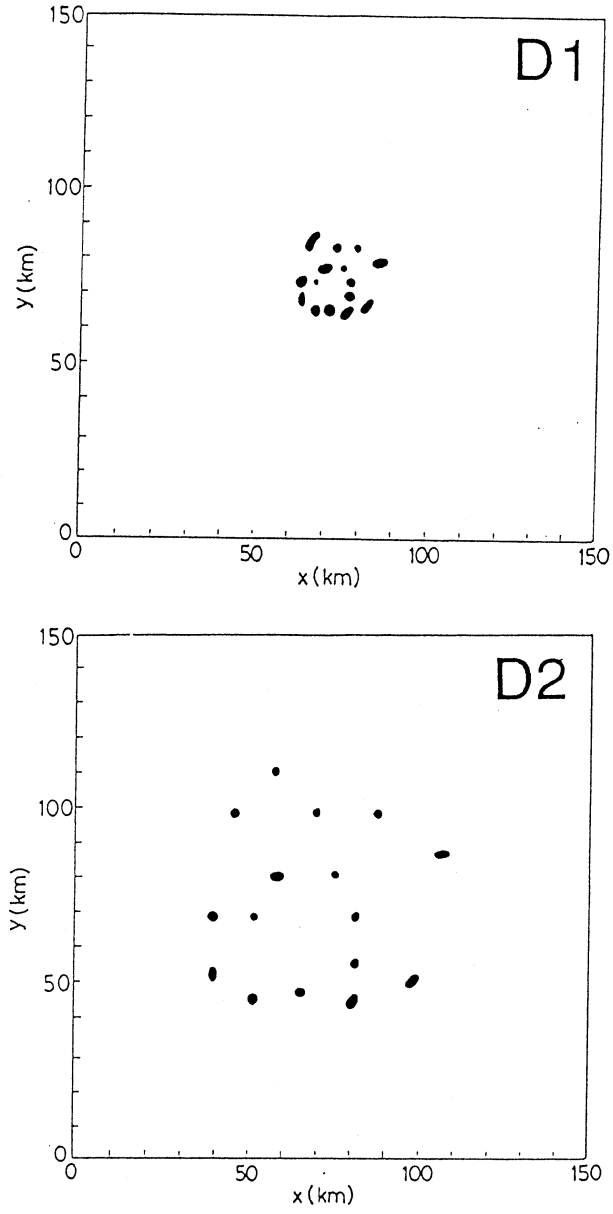

Fig. 3. Horizontal distribution of initial temperature deviations at 0.25 km level. Areas of temperature deviations larger than 0.5 K are shaded.

wind field could occur in a three-dimensional shear field, another type of vertical wind shear is given, as shown in Fig. 2b. Horizontal convergence or divergence due to large-scale air motion is not included in any of the cases.

Many small thermals are given as the initial disturbances in order to simulate a cluster of convective cells. Two types of initial disturbances are shown in Fig. 3. In the first type of disturbance, D1, thermals of positive temperature deviations less than 1.5 K are inserted at random places in a region of 30 km diameter at the 0.25 km level. In the second type of disturbance, D2, the same number of thermals is inserted into a region of 90 km diameter.

The values of the parameters in each case are shown in Table 1. Case A is a control case. The effects of changing the value of each parameter (the arrangement of the initial disturbance, ambient wind shear, or the instability of the atmosphere) will be studied by comparing the result of Case A with B, C, and D. The Bulk Richardson number in each case is also shown in Table 1. The values in Cases A and B are in the middle range between a multi-cell and supercell storms according to Weisman and Klemp (1982). Cases C1 and C3 are in the range of a multicell storm, and Cases C2 and D are in the range of a supercell storm. Numerical computation was made for 150 minutes in Case C3, and 120 min in the other cases.

3. Results of case A

3.1 Behavior of cells

Thermals given as the initial disturbance developed into precipitating convective cells. All of these cells produced precipitation. Figure 4 shows the horizontal distributions of the vertically-integrated precipitating-water content. Precipitating water found at 45 min was produced in these cells. After they decayed in several tens of minutes, many precipitating cells formed and decayed. At 120 min, precipitating water was distributed in bands. These bands consist of several precipitat-

Table 1. Values of parameters.

case	Temperature lapse rate from 1.75 km to 10.75 km level (°C/km)	Vertical wind shear below 9.75 km level (ms^{-1}/km)	Initial disturbance	bulk Richardson Number
A	7	2	D1	42
B	7	2	D2	42
C1	7	1	D1	84
C2	7	3	D1	19
C3	7	*1.7	D1	67
D	6	2	D1	33

* Containing veering in vertical wind shear below 3 km level

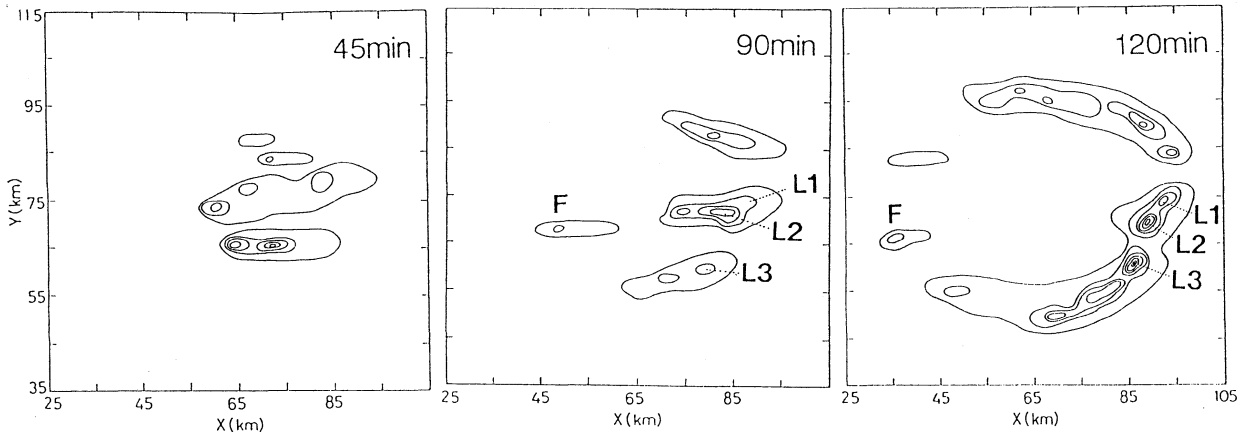

Fig. 4. Horizontal distributions of vertically - integrated precipitating-water content. The outermost contour indicates the content of 1 kg/m^2 , and contours are drawn every 5 kg/m^2. The symbols F and L denote typical F-type and L-type cells, respectively.

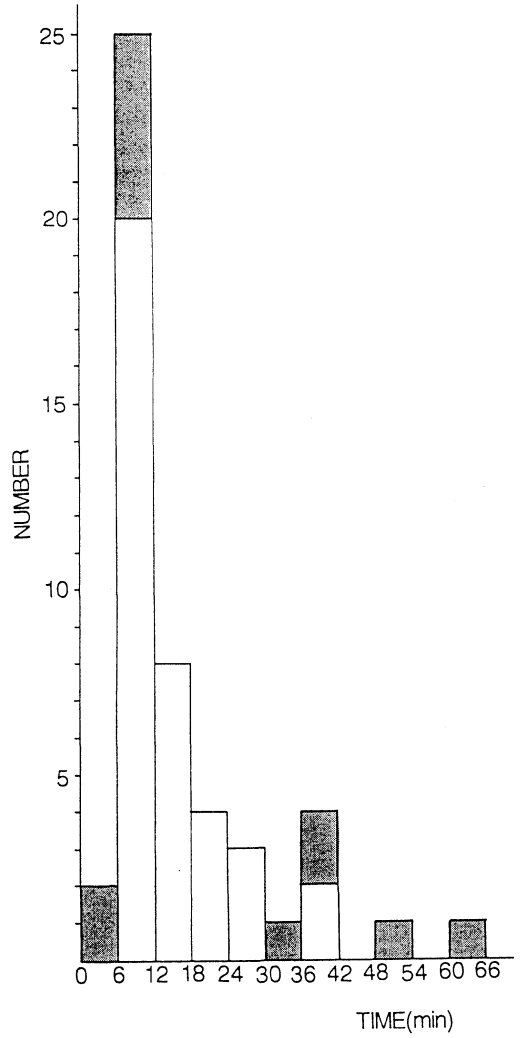

Fig. 5. Frequency distribution of the duration time of cells in case A. The cells which existed still at 120 min are shown by the shaded areas.

ing convective cells. Here, a precipitating convective unit, in which the intensity of an updraft exceeded 1 m/s at the 5.25 km level, is identified as "a cell".

Figure 5 shows the frequency distribution of the life-time of precipitating convective cells. The life-time of each cell is defined by the duration time of an updraft stronger than 1 m/s at the 5.25 km level. Almost half of the cells vanished in 6 to 12 minutes, but some cells persisted for several tens of minutes. Because the initial condition of the atmosphere was uniform in the horizontal direction, it is suggested that the different life-times of the cells originated from their interaction.

All of the cells are classified into three types according to their behavior and structure. The first type (S-type) is short-lived and shows the tilting of its updraft in the direction of vertical wind shear (so-called, downshear-tilting). The second type (F-type) is forced by the other cells and persists for a long time, although it has similar airflow structure to S-type. The third type (L-type) is long-lasting and it has an updraft which tilts against the direction of the vertical wind shear (so-called, upshear-tilting).

3.2 Structure of each type of cell

In the S-type cell the accumulation of precipitating-water and the formation of a downdraft occurs on the downshear side of the updraft. Because the downdraft cuts the surface flow which supplies warm and moist air into the updraft, the cell's life-span is short. Most of the cells belong to this type.

The vertical cross sections of a typical F-type cell is shown in Fig. 6. This cell is denoted by F in Fig. 4. An updraft tilts in the direction of vertical wind shear (left to right) while a downdraft exists to the downshear side of the updraft. The distribution of the updraft and downdraft are the same arrange-

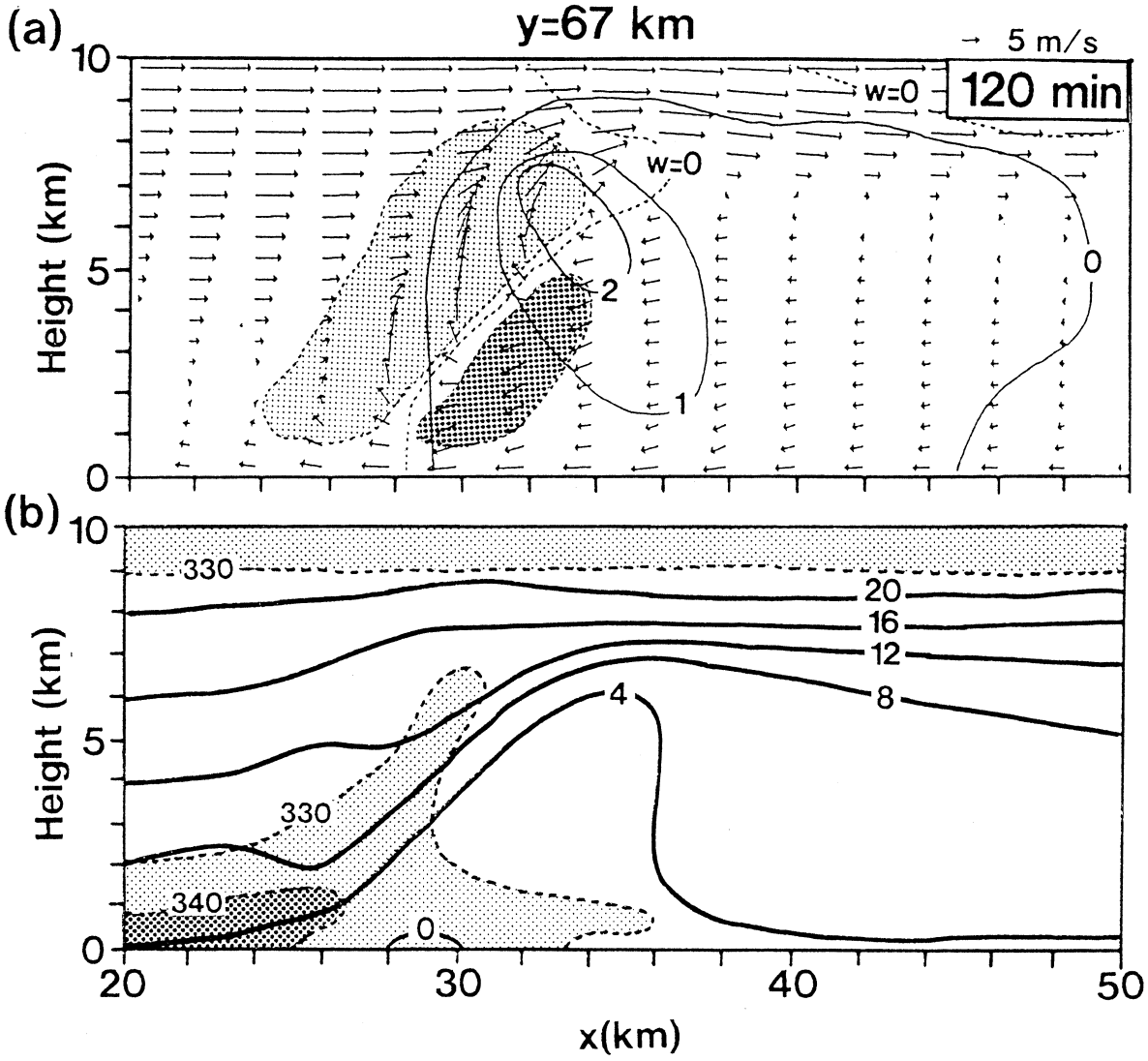

Fig. 6. Vertical cross sections of an F-type precipitating convective cell, which is denoted by F in Fig. 4. (a) Contours of Qp (solid lines; g/kg) and w (dashed lines). The dark and light shaded areas indicate updraft and downdraft stronger than 2 m/s, respectively. Vectors denote the wind component in the cross section. (b) Equivalent potential temperature (dashed lines; K) and horizontal wind velocity relative to the cell (solid lines; m/s).

ment as in S-type cells. But this cell continues to exist longer than fifty minutes past the end of the computation. Near the surface, especially around $x = 30$ km, the air moves very fast in the upshear direction and causes convergence at the foot of the updraft. As discussed in a later section, this strong flow is supplied by the other cells. The cell moves in the upshear direction very quickly relative to the domain, and the wind component relative to the cell is directed to the downshear side at almost all the levels (Fig. 6b). The distribution of equivalent potential temperature suggests that warm and moist air is supplied from the upshear side into the updraft. Thus the downdraft does not cut surface inflow into the updraft. Only four convective cells are classified into this type. All F-type cells were located at the upshear-side edge of the cell-cluster.

The vertical cross sections of a typical L-type cell are shown in Fig. 7. The common features of the L-type cells are the upshear tilting of the updraft and the accumulation of precipitating water to the upshear side (Fig. 7a). This arrangement of the updraft and the downdraft is just opposite to that of the S- or F-type cells. The air in the downdraft strongly diverges in the positive x-direction near the surface with the help of upper-level horizontal momentum. It collides vigorously with ambient wind and sustains the upshear-tilting updraft by pushing warm and moist air coming from the downshear side (Fig. 7b). Because the downdraft exists to the upshear side of the updraft, it does not cut the surface flow from the downshear side. This airflow structure

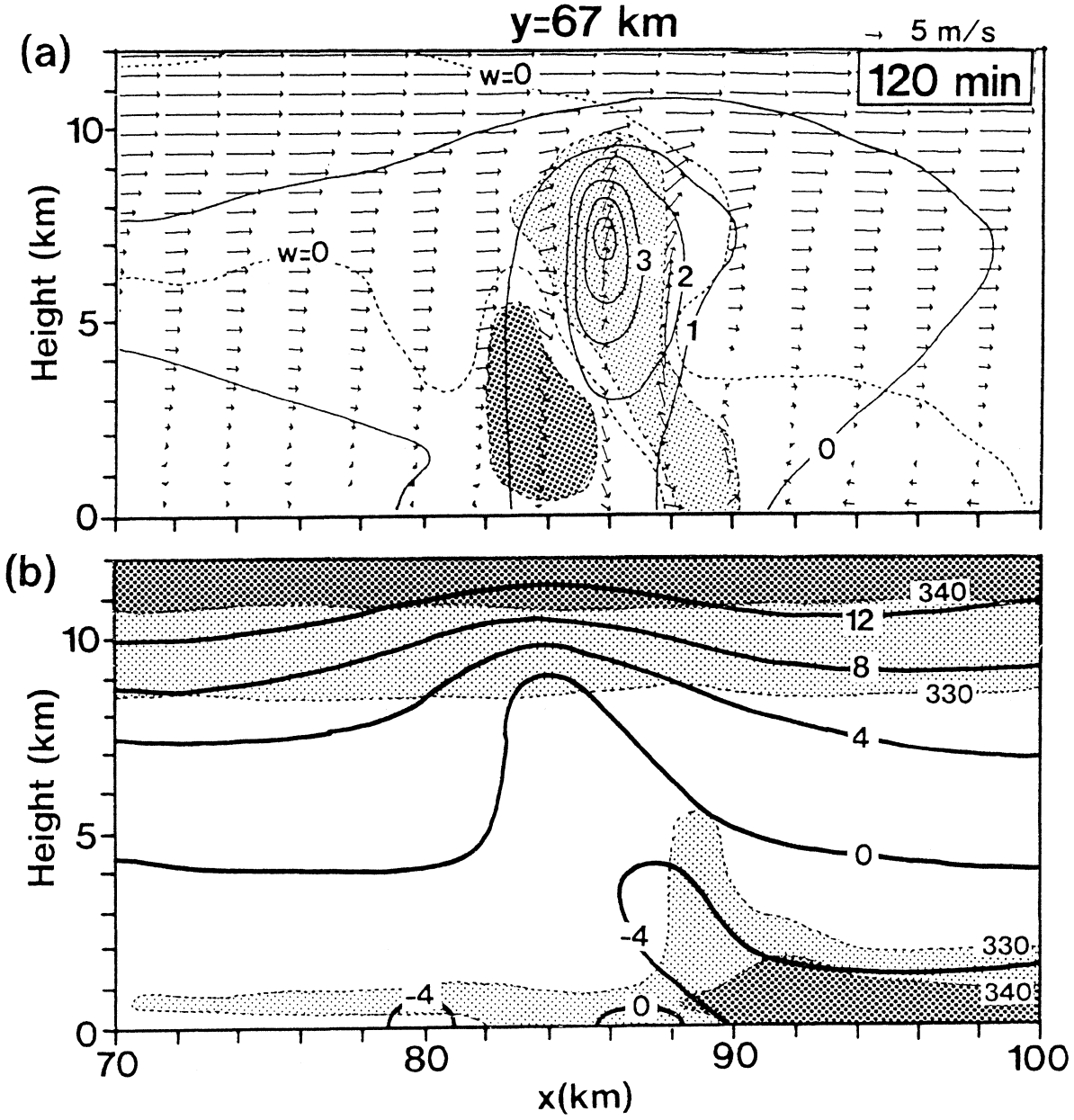

Fig. 7. Same as in Fig.6, except for an L-type cell denoted by L2 in Fig. 4.

is favorable for the maintenance of a convective cell (Browning and Ludlam, 1962). In case A, only three cells are classified as L-type (L1, L2 and L3 in Fig. 4).

3.3 Formation of L-type cells

In this section we will discuss how only three cells developed into L-type cells among many other types of cells. Figure 8 shows the horizontal sections of w and horizontal wind vectors around L-type cells. At the 0.25 km level, the narrow band-shaped updraft is found at the right side of the downdraft. The updraft and the downdraft in each cell are not always distributed parallel with the direction of the vertical wind shear. Strong flow diverging from the downdraft collides with the surrounding air at the right edge of the updraft area. At the 5.25 km level the updraft is divided clearly into the cells. Figures at the two levels show the updraft in each cell tilts in the upshear direction.

The time variation of updraft axes in the formation stage of L3 is shown in Fig. 9. Here the root of the axis is defined as the position of the updraft at the 1.5 km level. The updraft already tilts in the upshear direction at 81 min. Its tilting results from the difference between the horizontal velocity of the updraft root and the updraft top. The updraft root has an average rightward velocity of 6.9 m/s, while the updraft top (rising air parcel) moves at 2.8 m/s. The fast movement of the updraft root is essential

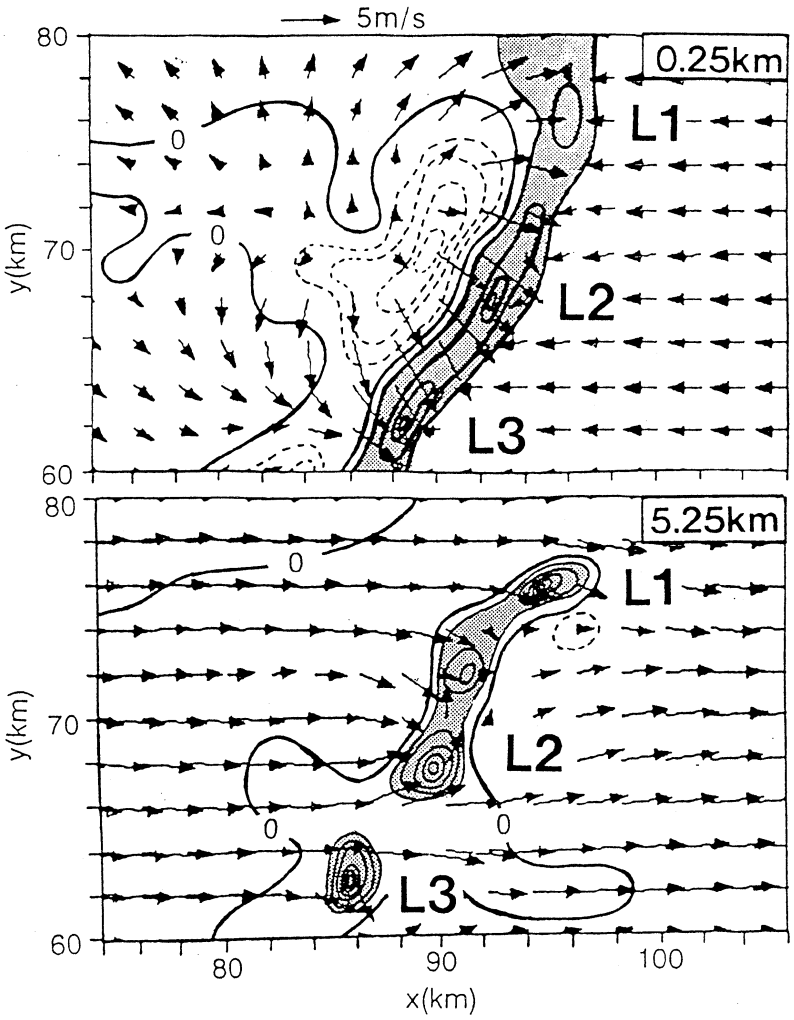

Fig. 8. Horizontal sections of w and horizontal wind vectors. Contours of w are drawn every 0.5 m/s at the 0.25 km level and 2 m/s at the 5.25 km level. Updrafts and downdrafts are drawn by solid and dashed lines, respectively. Dark shaded areas represent an updraft stronger than 0.5 m/s at 0.25 km, and 2 m/s at 5.25 km.

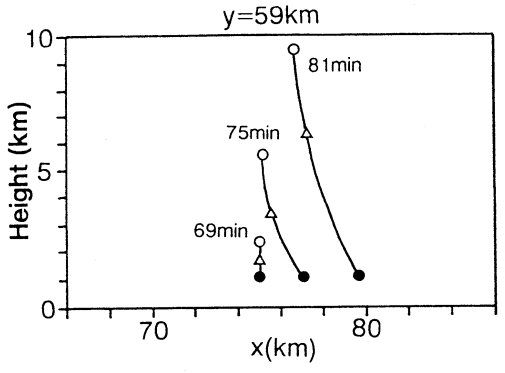

Fig. 9. Time variation of the updraft axes at $y = 59$ km. Solid lines show the position of the largest vertical velocity at each level. ● denotes the position of the largest vertical velocity at 1.5 km level, △ is the position of maximum vertical velocity and ○ is the highest position of the updraft stronger than 2 m/s.

for the upshear tilting of the updraft. This feature is common in the formation stage of all the L-type cells.

It is necessary to make clear how the updraft root moved fast in the downshear direction in the formation stage of the L-type cells. Figure 10 shows the time variations of w and horizontal wind vectors at the 0.25 km level. The updraft area at $y = 72$ km extends rightward (in the downshear direction) from 54 min to 66 min. Its right edge moved rightward by 5 km in this period. This movement corresponds to the fast shift of the updraft root. It can be seen from the figures that the successive outflow from the downdrafts of cells D, E and H caused the rightward extension of the updraft. At 54 min the outflow from cell D converges with the surrounding air around $x = 80$ km. From 60 min to 66 min, cells E and H, which are located to the downshear side of cell D, extends the updraft area to the right. L2 has formed at 78 min.

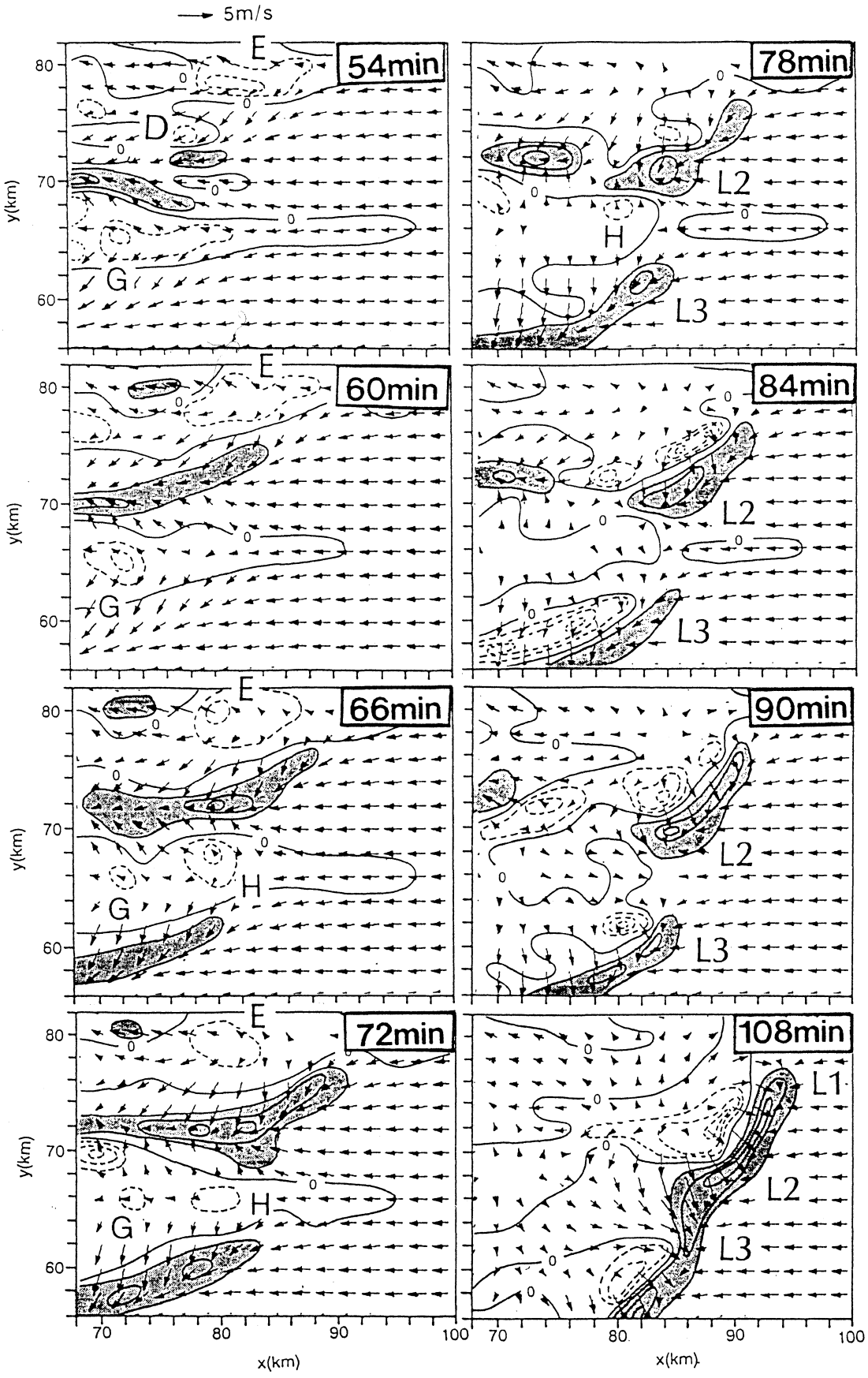

Fig. 10. Horizontal sections of w and horizontal wind vectors at the 0.25 km level. Updrafts and downdrafts stronger than 0.5 m/s are represented by dark shades and broken-lines, respectively.

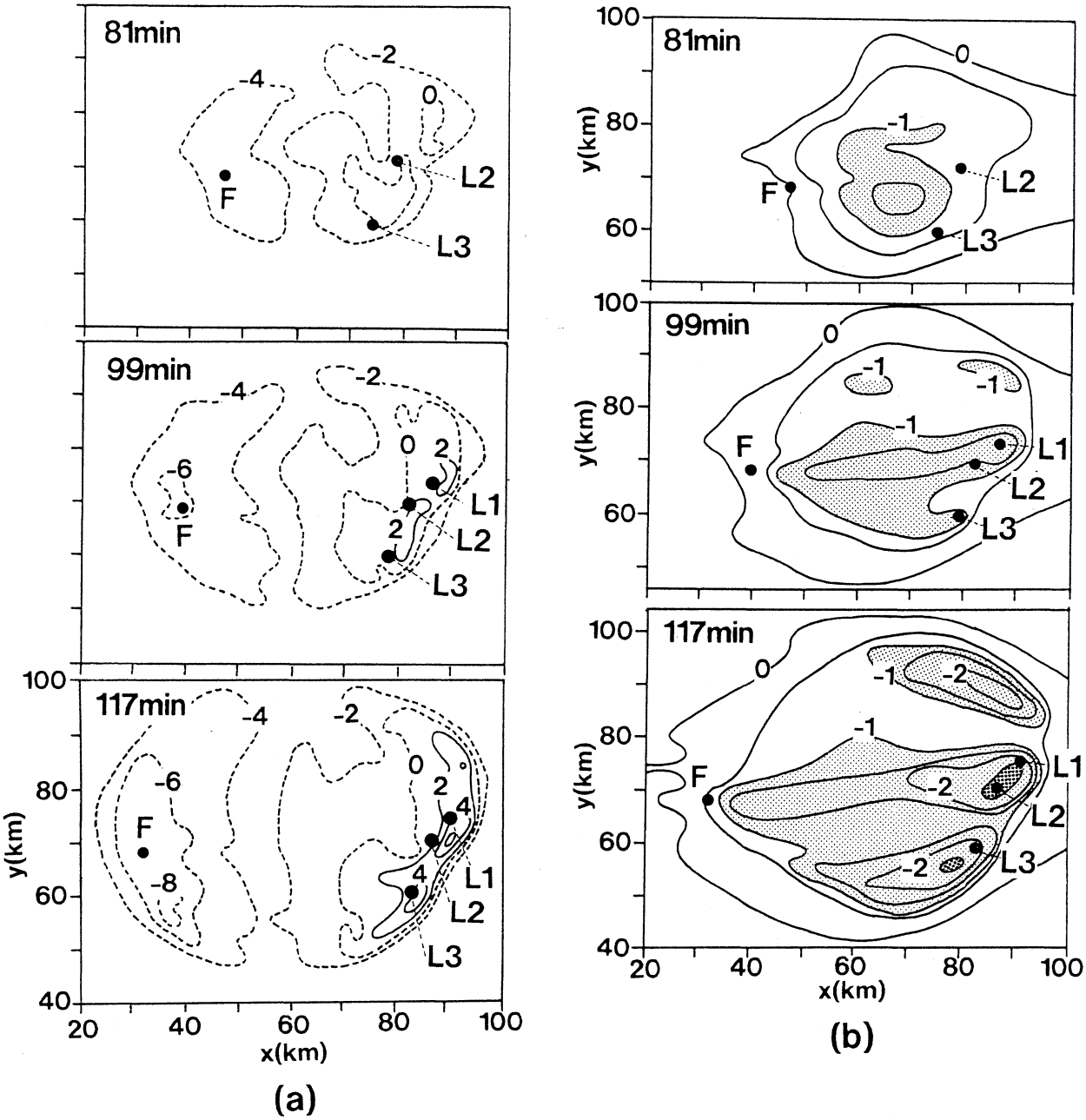

Fig. 11. Horizontal sections at the 0.25 km level of (a) u-component (contoured at 2 m/s intervals), (b) θ' (contoured at 0.5 K intervals; Dark and light shaded areas represent $\theta' < -2.5$ K and $\theta' < -1$ K, respectively) and (c) π' (contoured at 0.5×10^{-4} intervals; Dark and light shaded areas represent $\pi' > 1 \times 10^{-4}$ and $\pi' > 2 \times 10^{-4}$, respectively). Black spots denote the location of the maximum updrafts of F- and L-type cells at the 5.25 km level.

A similar rightward movement of the updraft root occurred at $y = 60$ km in relation to the outflow from cells G and H. L3 had already formed at 84 min. On the other hand, in the case of the formation of L1, the updraft root moved fast in the downshear direction with the help of the strong outflow supplied continuously from L2 (see from 84 min to 108 min).

In order to keep the upshear-tilting updraft for a long time, its root must keep on moving in the downshear direction. Figure 11a shows the horizontal distribution of u-component at the 0.25 km level. It is smaller than 2 m/s at any place at 81 min, although L2 and L3 have already formed. A u-component smaller than 2 m/s is too weak to keep the updrafts tilted in the upshear direction. At this time the upshear-tilting updrafts are sustained by the other cells as shown in Fig. 10. At 99 min u-components are intensified near the L-type cells and the local maxima exceed 2 m/s. At 117 min they

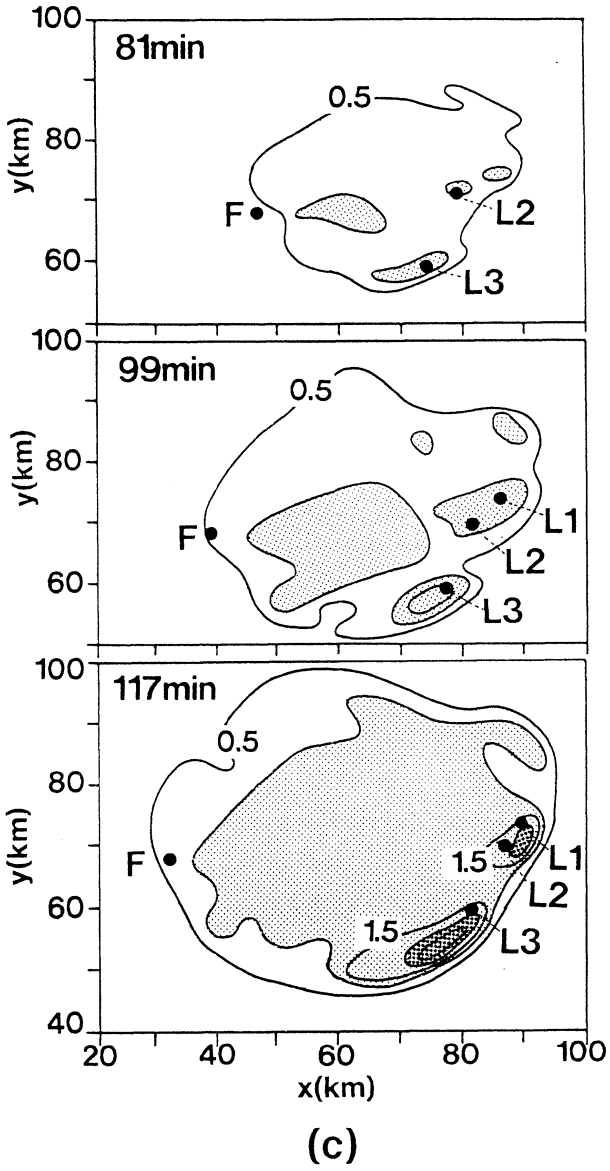

Fig. 11. (continued)

exceed 5 m/s. This value is large enough to keep the updrafts tilted to the upshear direction because it is larger than the rightward velocity of rising air parcels shown in Fig. 9. At this time the cells are self-maintained.

Figure 11b shows the horizontal distribution of θ' at the same level. A large pool of cold air is found at 81 min. At 99 min the area of $\theta' < -1$ K form near the L-type cells. At 117 min the areas of $\theta' < -2.5$ K are found only at the foot of the L-type cells. The extremely cool air is produced by continuous precipitation from the L-type cells. The distribution of π' (Fig. 11c) shows an extremely large value in the lower layer of L-type cells after 99 min.

The time variations shown in Fig. 11 indicate that cold outflow near the surface is locally intensified once an upshear-tilting updraft is built. This is caused by intensive evaporative cooling of continuous precipitation from the upshear-tilting updraft. In the mature stage of L-type cells, the updraft roots move with the strong outflow. The upshear-tilting updrafts must be sustained by the other cells until the cold outflows become strong enough to keep the updraft tilt to the upshear side.

3.4 Maintenance of F-type cells

F-type cells persisted for a long time although their airflow structure was similar to S-type cells. The important point in their maintenance is that the air moved very fast in the upshear direction near the surface (Fig. 6). The horizontal distribution of the u-component at the 0.25 km level (Fig. 11a) shows the existence of strong leftward winds on the upshear-side edge of the cell-cluster. The strong winds are found in a much broader area than the size of one cell. Figure 11c shows the existence of a pressure gradient from $x = 30$ km to $x = 40$ km at 117 min. The distribution of cold air is consistent with that of the high pressure. Around the F-type cells, the dynamic pressure at 0.25 km is much smaller than the hydrostatic pressure (not shown). It can be said that the large surface pressure gradient around F-type cells mainly resulted from the hydrostatic effect of the cold air. The large pool of cold air is maintained by the evaporation of precipitating water from convective cells which developed successively in the central region of the cell-cluster.

The maintenance process of an F-type cell can be summarized as follows. In the lower layer of F-type cells, the air moves very fast in the upshear direction due to the large pressure gradient which is maintained by successively-developed cells, and it collides vigorously with the surrounding warm and moist air near the root of the updraft. This updraft moves fast in the upshear direction together with the leading edge of the cold air. It can be said that an F-type cell is not self-maintained, but it is forced by cold outflows from neighboring cells.

4. Results of the other cases

In order to study the effects of various conditions on the formation process of long-lasting cells, numerical experiments were carried out for several other cases shown in Table 1. The horizontal distributions of the vertically-integrated precipitating water amount at 120 min in each case are shown in Fig. 12.

4.1 Case B

Initial thermals in Case B were more scattered than in Case A. As a result, precipitating cells formed at a greater distance from each other than in case A. In this case, such a process as in Fig. 10 did not occur because the cells were too distant from each other. No L-type cell was found until the end of the computation. Figure 13 shows the

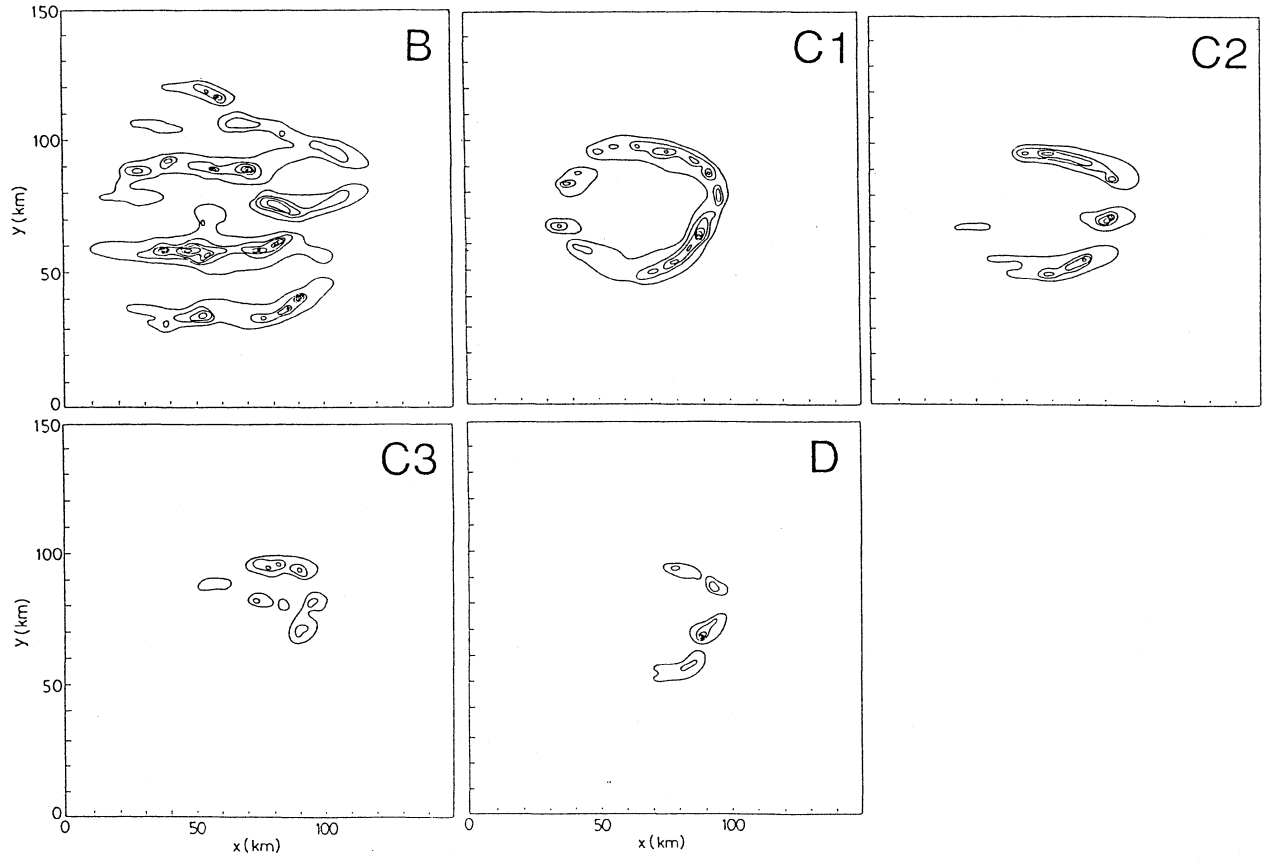

Fig. 12. Horizontal distributions of vertically-integrated precipitating water content at 120 min in cases B, C1, C2, C3 and D. Outermost contours correspond to 1 kg/m^2, and the contours are drawn every 5 kg/m^2.

horizontal distribution of the u-component at the 0.25 km level at 120 min. Its maximum value is less than 4 m/s, while it exceeded 6 m/s in Case A (see Fig. 11a). Neither extremely cold air nor high pressure was found in this case. This result indicates the importance of the interaction patterns shown in Fig.10 in the product of the strong cold outflow which maintains an L-type cell. Seven F-type cells are found in this case.

4.2 Cases C1 and C2

In Case C1 weaker vertical wind shear was given initially. Four L-type cells formed in this case. But these cells formed through a rather different process than Case A. As seen in Fig. 14, the downdraft from Cell I collides with the surrounding air. As the updraft area is shifted in the downshear direction only in association with the evolution of the S-type Cell I, the upshear-tilting updraft is built and an L-type cell forms. In Case C1, seven F-type cells formed on the upshear-side of the cold air pool in the same way as in Case A.

In Case C2, stronger vertical wind shear was given initially. As a result, only one L-type cell formed through almost the same process as L2 in Case A. However, some cells failed to become L-type cells because the vertical wind shear was too strong for their updrafts to tilt to the upshear direction. Three F-type cells were found in this case.

4.3 Case C3

In Case C3 the direction of the ambient wind shear turns below the 3 km level (Fig. 2b). This case was set up in order to examine whether the process found in the unidirectional wind cases could occur in a three-dimensional shear field. In Fig. 15 Cell J is an L-type cell. Its updraft tilts in the negative x-direction. At the 0.25 km level its updraft and downdraft are distributed almost along the x-axis with some angles to the direction of the vertical wind shear below the 3 km level. The formation process of Cell J was similar to that of Cells L2 or L3 in Case A. Cells K and M are of the F-type. Both cells are located at the edge of the cold pool at the 0.25 km level, and they showed similar behavior to the F-type cells in Case A.

4.4 Case D

The initial atmosphere in Case D is more stable than in Case A. In this case only one L-type cell formed at the location where Cell L2 was found in Case A. Its formation process was similar to that of

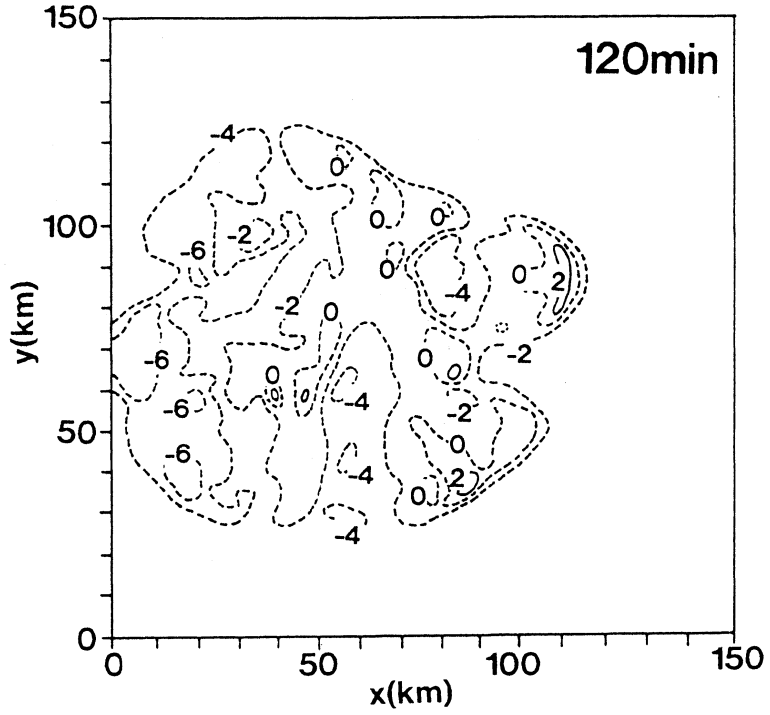

Fig. 13. Horizontal sections of the u-component at the 0.25 km level in case B at 120 min. Contours are drawn every 2 m/s.

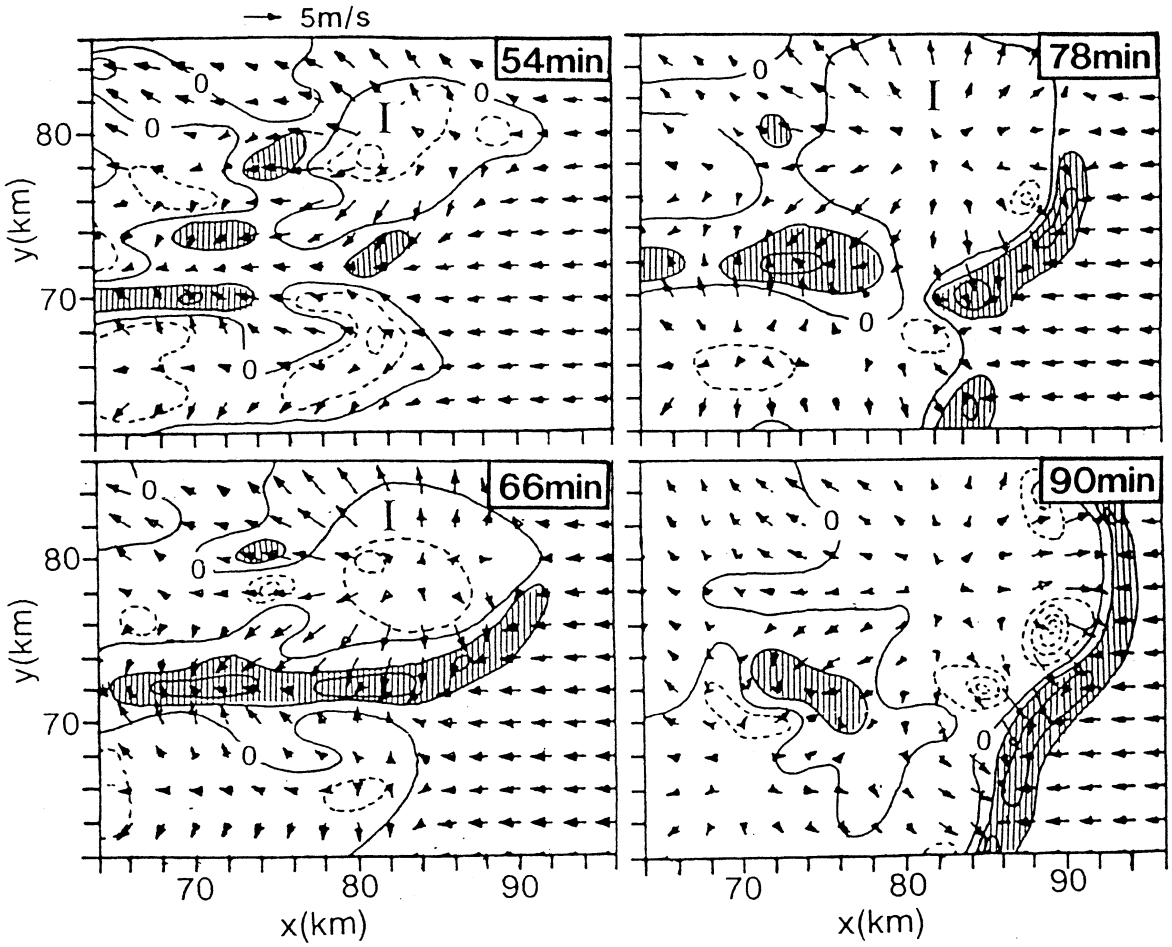

Fig. 14. Same as Fig.10, except for case C1.

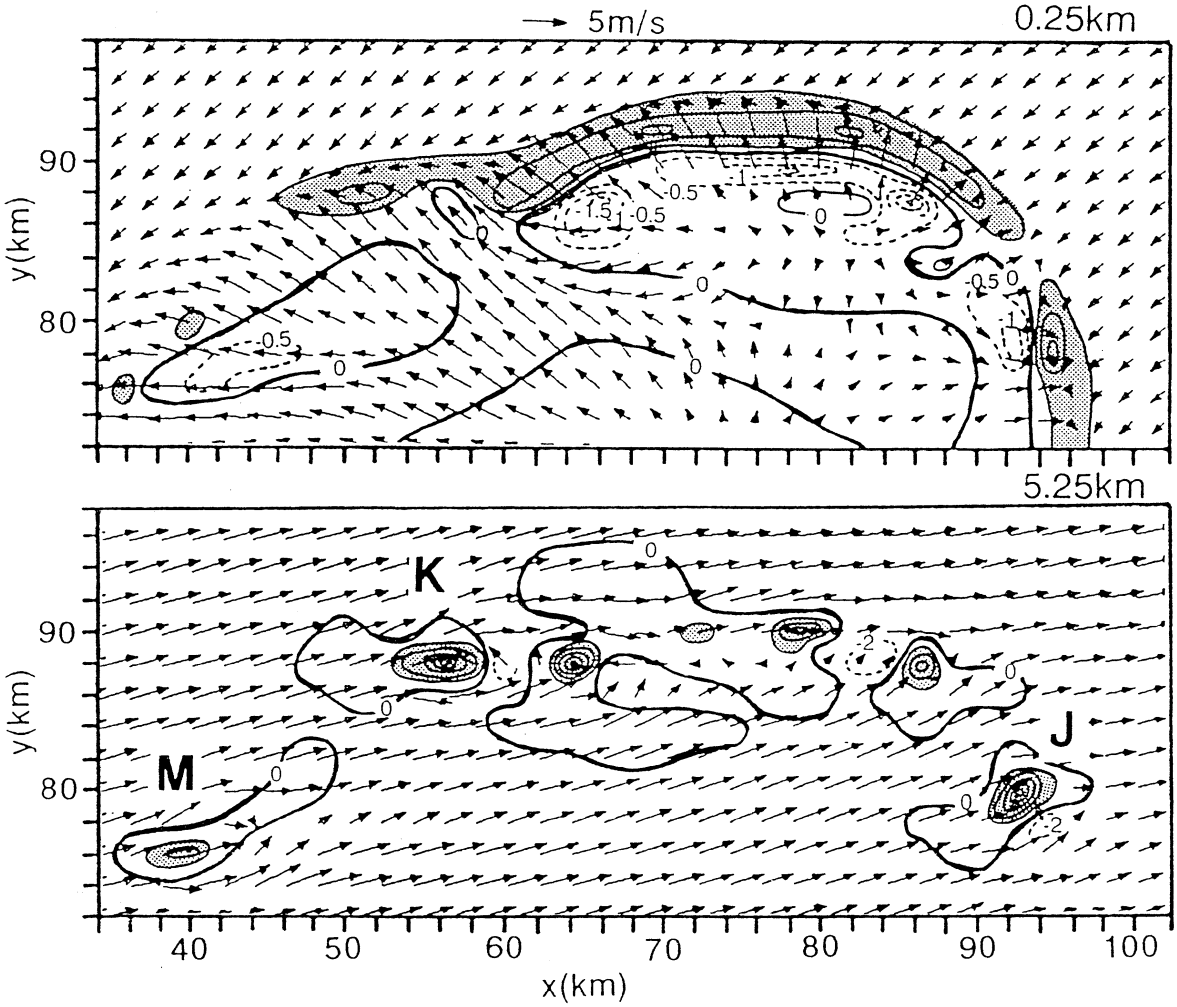

Fig. 15. Same as Fig.8, except for case C3.

L2. No F-type cells formed in this case, since the atmosphere was too stable to produce precipitation on the upshear-side edge of the cold air pool. This result suggests that the formation of an F-type cell is sensitive to the instability of the atmosphere.

5. Discussion

Various types of precipitating convective cells developed in each case of computation. The types of cells were classified into three types; S, F and L. Because the initial conditions were horizontally homogeneous in each case, this variability resulted from interactions of the convective cells. The formation of long-lasting cells is discussed herein.

The upshear-tilt of an updraft is essential for the formation of L-type cells. In order to make the updraft tilt against the direction of the vertical shear, the updraft root must move in a downshear direction faster than the rising air parcels. Roughly speaking, its critical speed is the averaged horizontal velocity of the ambient wind in the layer from the surface to the top. The critical speed is smaller when the ambient vertical wind shear is weaker.

The fast movement of the updraft root was forced by the other cells in the formation stage of L-type cells. Three patterns were found in this process as is shown schematically in Fig. 16. In Pattern I the updraft root moved with the outflow diverging from one short-lived cell. This pattern was found when the vertical wind shear was weak (Case C1). Because the critical speed of the updraft root is small when the vertical wind shear is weak, it is probable that one short-lived cell supplies enough outflow to produce an upshear-tilting updraft. In Pattern II it moved with the outflow boundaries of several short-lived cells which formed successively. As shown in Case A, this pattern can be found when the cells are sufficiently adjacent to each other. In Pattern III the updraft root moved together with the outflow diverging from a pre-existing L-type cell. This pattern was found in the formation of Cell L1 in Case A. It is considered that this pattern can be found when the surface convergence zone produced by a pre-existing L-type cell covers a very wide area. Once an upshear-tilting updraft is built through the processes, a strong cold-air pool is produced near

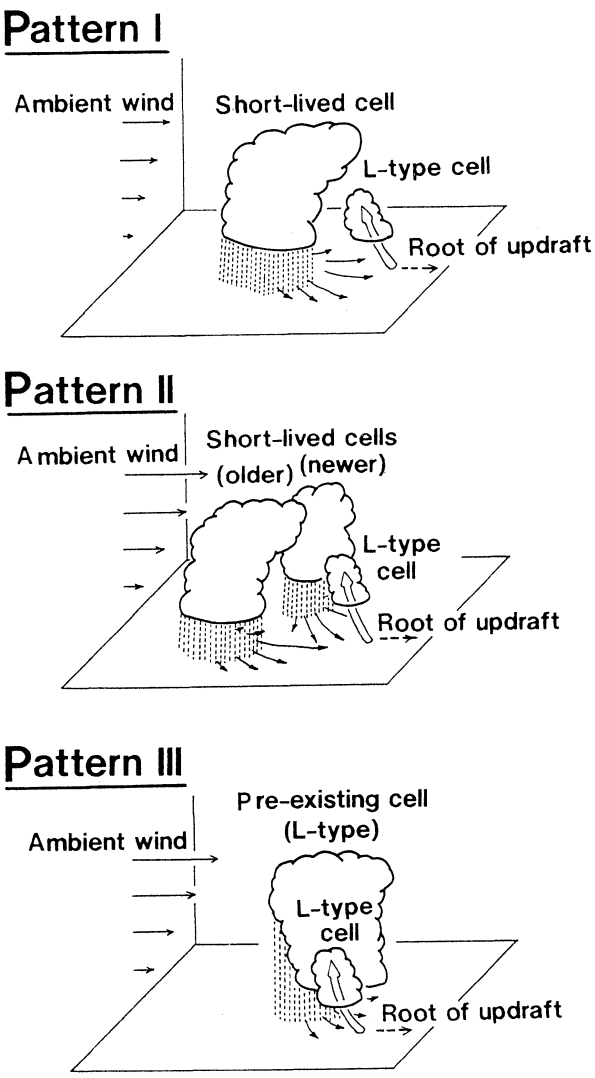

Fig. 16. Three patterns of the rôle of the other cells in the formation of the upshear-tilting updraft.

the surface by evaporation of continuous precipitation from the updraft. The L-type cell can be self-maintained after the formation of the strong cold-air pool.

Most of the observations of convective clouds focus on the structure of their mature stage, and there are very few studies on the formation stage of long-lasting clouds. Takeda and Imai (1976) analyzed the formation stage of a long-lasting convective echo. They found differences in the developing stage in two adjacent convective echoes just before the formation of the long-lasting echo. This implies the occurrence of Pattern II, but there were no data to analyze the cloud-scale wind field. Accumulation of more observational data is needed to support the results of the present study.

Figure 17 shows schematically the maintenance process of the F-type cell. Its updraft is sustained by a strong convergence caused by cold air which moves very fast in the upshear direction. The cold air at the foot of the F-type cell is accelerated in the upshear direction by the pressure gradient at the surface. The cold-air pool is produced by evaporative cooling of water precipitating from the pre-existing convective cell ensemble. The existence of the other cells is indispensable for the maintenance of F-type cells.

In the real atmosphere, convective clouds which show a very similar behavior to F-type cells are often observed. For example, Knupp and Cotton (1987) observed multi-cellular convective echoes which propagated in the upshear direction. These echoes were located at the upshear-side edge of a meso-scale echo-cluster, and successively developed echoes were observed at the other edge of the cluster.

6. Summary

In order to study the formation process of long-lasting precipitating convective cells, a three-dimensional numerical simulation of convective-cloud ensemble was performed. As the initial condition, random small thermals were given in the horizontally homogeneous atmosphere.

Three types of cells developed in the numerical domain. The first type (S-type) had a downshear-tilting updraft and was short-lived. Most of the cells belonged to this type. The second type (F-type) showed a similar airflow structure to the S-type, but was forced by cold outflows from the other cells and persisted for a long-time. The third type (L-type) had an upshear-tilting updraft and it was self-maintained. Because the initial condition was horizontally homogeneous, this variability in the behavior resulted from the interactions of precipitating convective cells. The formation patterns of long-lasting cells were discussed.

In the formation process of an L-type cell, its updraft root must move faster than rising air parcels. The fast movement of the updraft root was initially forced by the other cells. The results showed there are three patterns in this process. In Pattern I, the updraft root moves with outflow diverging from one short-lived cell. This pattern occurred when the ambient vertical wind shear was weak. In Pattern II, the updraft root moves with outflow boundaries of several short-lived cells which form successively. This pattern occurred when the cells were sufficiently adjacent to each other. In Pattern III, the updraft root moves together with outflow diverging from a pre-existing L-type cell. Once an upshear-tilting updraft is built through these processes, an intensive cold-air pool is produced near the surface and the cells are self-maintained at its edge.

One of the most interesting results in this paper is that several short-lived cells contribute to the for-

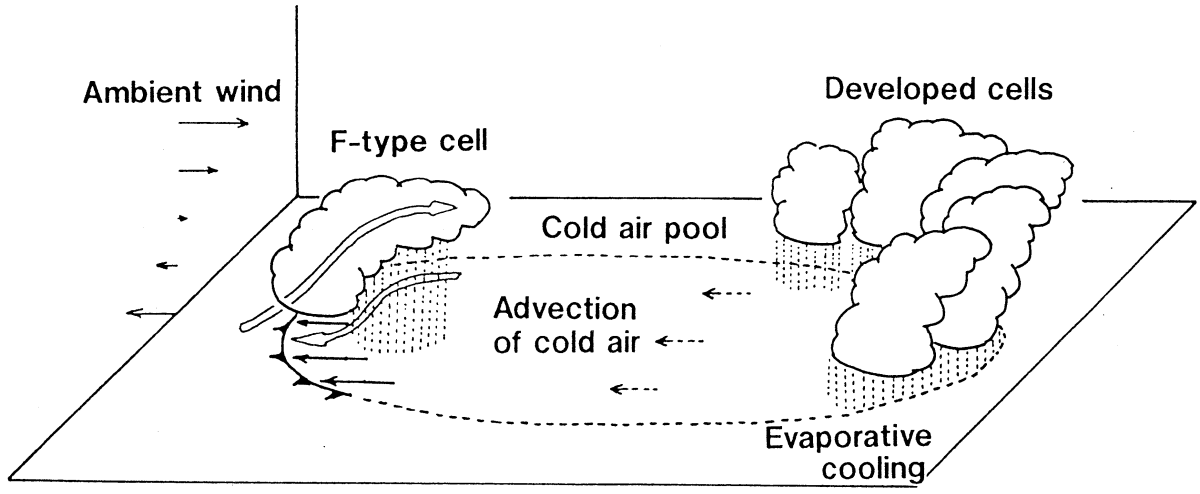

Fig. 17. Schematic representation of the maintenance of an F-type precipitating convective cell.

mation of one long-lasting cell. In the numerical simulation of long-lasting cells, very large isolated thermals were often given as the initial disturbances. In a cluster of convective cells, it is considered that several short-lived cells play the rôle of such an artificial large isolated thermal.

This study showed the formation patterns of long-lasting cells under the situation in which convective-cell interactions exist. But the model does not include mesoscale disturbances or orographic effects. The formation patterns in a more realistic atmosphere must be studied as the next step.

Acknowledgments

The authors wish to express their hearty thanks to Dr. Y. Fujiyoshi and Dr. K. Kato of Nagoya University for their useful and stimulating discussions. The authors are deeply grateful to two anonymous reviewers for improving the original manuscript. Numerical calculations were carried out by using FACOM M-780 computers of Nagoya University.

Appendix

A. Equations used in the numerical model

All the symbols in the following equations are explained in Appendix B. Symbols with upper bars denote a basic state which is dependent only on the height, and dashed symbols mean a deviation from the basic state.

The three-dimensional equations of motion are written as:

$$\frac{\partial \boldsymbol{V}}{\partial t} = -(\boldsymbol{V}\cdot\nabla)\boldsymbol{V} - c_p\bar{\theta}\pi' + \boldsymbol{k}g\left\{\frac{\theta'}{\bar{\theta}} + 0.61Q'v - Qc - Qp\right\} + \boldsymbol{k}\nabla^2\boldsymbol{V}'. \quad \text{(A.1)}$$

The continuity equation is,

$$\nabla(\bar{\rho}\boldsymbol{V}) = 0. \quad \text{(A.2)}$$

The diagnostic equation of pressure can be deduced from equations (A.1) and (A.2) as follows:

$$c_p\nabla\bar{\rho}\bar{\theta}\nabla\pi' = -\nabla\left\{\bar{\rho}(\boldsymbol{V}\cdot\nabla)\boldsymbol{V} - \bar{\rho}\kappa\nabla^2\boldsymbol{V}'\right\} + \frac{\partial}{\partial z}\left\{\bar{\rho}g\left(\frac{\theta'}{\bar{\theta}} + 0.61Q'v - Qc - Qp\right)\right\}. \quad \text{(A.3)}$$

The prognostic equations of potential temperature and water substances are given by:

$$\frac{\partial\theta}{\partial t} = -(\boldsymbol{V}\cdot\nabla)\theta + \frac{L}{c_p\bar{\pi}}(P1 - P2) + \kappa\nabla^2\theta', \quad \text{(A.4)}$$

$$\frac{\partial Qv}{\partial t} = -(\boldsymbol{V}\cdot\nabla)Qv - P1 + P2 + \kappa\nabla^2Q'v, \quad \text{(A.5)}$$

$$\frac{\partial Qc}{\partial t} = -(\boldsymbol{V}\cdot\nabla)Qc + P1 - P3 + \kappa\nabla^2Qc, \quad \text{(A.6)}$$

$$\frac{\partial Qp}{\partial t} = -(\boldsymbol{V}\cdot\nabla)Qp - P2 + P3 + \frac{1}{\bar{\rho}}\frac{\partial}{\partial z}(\bar{\rho}VpQp) + \kappa\nabla^2Qp. \quad \text{(A.7)}$$

$P1$, $P2$ and $P3$ represent the transformation rate from water vapor into cloud water, the evaporation rate of precipitating water and the formation rate of precipitating water. All eddy-diffusion coefficients are constant, both temporarily and spatially. Their values are 200 m^2/s.

Transformation rate from water vapor into cloud water (P1)

Considering the release of latent heat, P1 is given by the following equation:

$$P1 = \alpha\left\{\frac{Qv - Qs}{1 + \frac{L}{c_p}\left(\frac{\partial Qs}{\partial T}\right)}\right\}. \quad \text{(A.8)}$$

α is the inverse of the transition time to the equilibrium state. Here its value is the inverse of one time-step.

Evaporation rate of precipitating water (P2)

The evaporation rate of a spherical water drop of diameter D and mass M is given by:

$$\frac{\partial M}{\partial t} = -2\pi_A D\left(\frac{Qv}{Qs}-1\right)\left\{\frac{L^2}{KaRvT^2}+\frac{RvT}{Dve_s}\right\}^{-1} Cv. \quad \text{(A.9)}$$

Cv represents a ventilation coefficient. Assuming that the size distribution of the water drop is given by the Marshall-Palmer distribution,

$$N_D dD = N_o exp(-\lambda D)dD, \quad \text{(A.10)}$$

P2 is given by:

$$P2 = \int\left(-\frac{\partial M}{\partial t}N_D\frac{1}{\rho}\right)dD = \frac{2\pi_A}{\rho}\left(1-\frac{Qv}{Qs}\right)\times N_o\left\{\frac{L^2}{KaRvT^2}+\frac{RvT}{Dve_s}\right\}^{-1} Cv\Gamma(2)\frac{1}{\lambda^2}. \quad \text{(A.11)}$$

Γ denotes the gamma function and N_o is constant. λ is the perameter given by:

$$\lambda = \left(\frac{\pi_A \rho_w N_o}{\bar{\rho} Qp}\right)^{0.25}. \quad \text{(A.12)}$$

The ventilation coefficient is approximated to be

$$Cv = 1 + 0.1Vp^{\frac{3}{2}}. \quad \text{(A.13)}$$

Formation rate of precipitating water (P3)

In the real atmosphere, the formation rate of precipitating water is variable with time and space dependently on temperature, the size distribution of cloud particles and other factors. In order to represent, here, only the most essential effects of precipitation-formation processes on the dynamics of a convective cloud, the formation rate of precipitating water is given very simply by

$$P3 = AQc + BQcQp. \quad \text{(A.14)}$$

The first and second terms in the right represent the conversion process of cloud droplets or small ice particles into precipitating particles, and the accretion process of cloud droplets or small ice particles to precipitating particles, respectively.

In a deep convective cloud, precipitating particles form often through ice-phase processes. The formation of precipitating water through ice-phase processes is represented simply by fixing the values A and B to be

$$\begin{cases} A = 0 & (\text{if } T > -20^\circ\text{C}) \\ A = 1.0\times 10^{-3} & (\text{if } T < -20^\circ\text{C}) \\ B = 4.0 \end{cases} \quad \text{(A.15)}$$

Falling velocity of precipitating water (Vp)

By assuming that the falling velocity of a precipitating drop of diameter, D, is denoted by $V_D = aD^b$, and that the size distribution of precipitating drops is represented by the Marshall-Palmer distribution, the mass-mean falling velocity of precipitating water is given by,

$$Vp = \frac{\int V_D \frac{\pi}{6} D^3 N_o exp(-\lambda D)dD}{\int \frac{\pi}{6} D^3 N_o exp(-\lambda D)dD} = \frac{\Gamma(4+b)}{6\lambda^b}, \quad \text{(A.16)}$$

Here, the parameters a and b are given by the experiment of Gunn and Kinzer (1949) as $842\,\mathrm{m}^{1-b}/\mathrm{s}$ and 0.8.

Computational scheme

For the advection of velocity and temperature, the forward difference scheme in time and upstream difference scheme in space are used. To prohibit the growth of an unstable gravity wave, the vertical advection term of the potential temperature at the time step n is evaluated using the vertical velocity at the time step $n+1$. For the advection of mixing ratios, the forward in time and flux-upstream difference scheme in space are used. For the diffusion term, the forward difference scheme in time and the centered difference scheme in space are used. The time step is fixed as 10 sec.

B. List of symbols

A, B	parameters in formation process of precipitating water	
a, b	parameters on falling speed of precipitating-drops	
c_p	specific heat of air	1.0×10^3 $\mathrm{J\,kg^{-1}\,K^{-1}}$
Cv	ventilation coefficient	
Dv	diffusivity of water vapor	2.3×10^{-5} $\mathrm{m^2\,s^{-1}}$
e_s	saturation vapor pressure	$\mathrm{Nm^{-2}}$

g	acceleration of gravity	9.8	ms^{-2}
Ka	thermal conductivity of air	2.4×10^{-2}	$\mathrm{Jm}^{-1}\,\mathrm{s}^{-1}\,\mathrm{K}$
L	latent heat of condensation	2.5×10^{6}	$\mathrm{J\,kg}^{-1}$
N_o	constant in parameterization of precipitating drop size distribution	8.0×10^{6}	m^{-4}
$N_D dD$	number concentration of precipitating drops of diameter $D \sim D + dD$		m^{-3}
P	pressure		Nm^{-2}
$P1$	transformation rate between water vapor and cloud water		$\mathrm{kg\,kg}^{-1}\,\mathrm{s}^{-1}$
$P2$	evaporation rate of precipitating water		$\mathrm{kg\,kg}^{-1}\,\mathrm{s}^{-1}$
$P3$	formation rate of precipitating water		$\mathrm{kg\,kg}^{-1}\,\mathrm{s}^{-1}$
Qc	mixing ratio of cloud water		$\mathrm{kg\,kg}^{-1}$
Qp	mixing ratio of precipitating water		$\mathrm{kg\,kg}^{-1}$
Qs	mixing ratio of saturated water vapor		$\mathrm{kg\,kg}^{-1}$
Qv	mixing ratio of water vapor		$\mathrm{kg\,kg}^{-1}$
Rv	gas constant of water vapor	461	$\mathrm{J\,kg}^{-1}\,\mathrm{K}^{-1}$
t	time		s
T	temperature		K
u	air velocity in x direction		ms^{-1}
v	air velocity in y direction		ms^{-1}
Vp	mass mean fall speed of precipitating water		ms^{-1}
w	air velocity in z direction		ms^{-1}
x	horizontal coordinate		
y	horizontal coordinate		
z	vertical coordinate		
α	inverse of transition from super-saturated state to equilibrium state		s^{-1}
Γ	gamma function		
κ	eddy diffusion coefficient	200	$\mathrm{m}^2\,\mathrm{s}^{-1}$
θ	potential temperature		K
λ	parameter in precipitating-drop size distribution		
π	non-dimensional pressure $\pi = (P/P0)^{R/c_p}$, $P0 = 1000\,\mathrm{hPa}$, $R/c_p = 0.286$		
π_A	geometric constant	3.1416	
ρ	density of air		$\mathrm{kg\,m}^{-2}$
ρ_w	density of liquid water		$\mathrm{kg\,m}^{-2}$

References

Balaji, V. and T.L. Clark, 1988: Scale selection in locally forced convective fields and the initiation of deep cumulus. *J. Atmos. Sci.*, **45**, 3188–3211.

Bluestein, H.B. and S.S. Parker, 1993: Modes of isolated severe convective storm formation along the dryline. *Mon. Wea. Rev.*, **121**, 1354–1372.

Browning, K.A. and F.H. Ludlam, 1962: Air flow in convective storms. *Quart. J. Roy. Meteor. Soc.*, **88**, 117–135.

Clark, T.L., 1979: Numerical simulations with a three-dimensional cloud model: Lateral boundary condition experiments and multicellular severe storm simulations. *J. Atmos. Sci.*, **36**, 2191–2215.

Fankhauser, J.C., 1971: Thunderstorm-environment interactions determined from aircraft and radar observation. *Mon. Wea. Rev.*, **99**, 171–192.

Fovell, R.G. and Y. Ogura, 1988: Numerical simulation of a midlatitude squall line in two dimensions. *J. Atmos. Sci.*, **45**, 3846–3879.

Gunn, R. and G.D. Kinzer, 1949: The terminal velocity of fall for water droplets in stagnant air. *J. Meteor.*, **6**, 243–248.

Knupp, K.R. and W.R. Cotton, 1987: Internal structure of a small mesoscale convective system. *Mon. Wea. Rev.*, **115**, 629–645.

Orlanski, I., 1976: A simple boundary condition for unbounded hyperbolic flows. *J. Comput. Phys.*, **21**, 251–269.

Schlesinger, R.E., 1980: A three-dimensional numerical model of an isolated thunderstorm: Part II. Dynamics of updraft splitting and mesovortex couplet evolution. *J. Atmos. Sci.*, **37**, 395–420.

Seitter, K.L. and H. Kuo, 1983: The dynamical structure of squall-line type thunderstorms. *J. Atmos. Sci.*,

40, 2831–2854.
Seko, K. and T. Takeda, 1987: Radar-echo structure of a quasi-steady heavy rain storm. *Natural Disaster Sci.*, **9**, 23–37.
Tabata, A., S. Nakazawa, Y. Yasutomi, H. Sakakibara, M. Ishihara and K. Akaeda, 1989: The structure of a long-lasting single cell convective cloud. *Tenki*, **36**, 499–507 (in Japanese).
Takeda, T., 1971: Numerical simulation of a precipitating convective cloud: The formation of a 'long-lasting' cloud. *J. Atmos. Sci.*, **28**, 350–376.
Takeda, T., and H. Imai, 1976: On the behavior of long-lasting cellular echoes. *J. Meteor. Soc. Japan*, **54**, 399–406.
Tao, W.K. and S.T. Soong, 1986: A study of the response of deep tropical clouds to mesoscale processes: Three-dimensional numerical experiments. *J. Atmos. Sci.*, **43**, 2653–2676.
Tao, W.K. and J. Simpson, 1989a: Modeling study of a tropical squall-type convective line. *J. Atmos. Sci.*, **46**, 177–202.
Tao, W.K. and J. Simpson, 1989b: A further study of cumulus interaction and mergers: Three-dimensional simulation with trajectory analysis. *J. Atmos. Sci.*, **46**, 2974–3004.
Weisman, M.L. and J.B. Klemp, 1982: The dependence of numerically simulated convective storms on wind shear and buoyancy. *Mon. Wea. Rev.*, **110**, 504–520.
Wilhelmson, R.B. and J.B. Klemp, 1978: A numerical study of storm splitting that leads to long-lived storms. *J. Atmos. Sci.*, **35**, 1974–1986.
Yoshizaki, M., 1978: Numerical experiments of a convective cloud with a high cloud base in shear flows. *J. Meteor. Soc. Japan*, **56**, 387–404.

組織化した対流性ストームの形成過程に関する数値的研究
第1部・長寿命セルの形成パターン

三隅良平[1]・Marjan Divjak[2]・棚橋修一[3]・武田喬男
(名古屋大学大気水圏科学研究所)

長寿命の降水性対流セルの形成過程を調べる目的で、積乱雲群の3次元数値シミュレーションを行った。初期条件として、水平方向に一様な大気場に、小さいサーマルをランダムに与えた。

形成した対流セルは、次の3つの型に分類された。第1の型 (Sタイプ) のセルは短寿命で、鉛直シアーの風下に傾いた上昇流を持つ。第2の型 (Fタイプ) はSタイプと同じ気流構造を持つが、他のセルによって強制されることにより長続きする。第3の型 (Lタイプ) は長寿命で、鉛直シアーの風上に傾いた上昇流を持つ。

Lタイプのセルの形成過程において、上昇流がシアーの風上側に傾くためには、上昇流の根が上昇する空気魂よりも速くシアーの風下側に移動せねばならない。その形成段階では、隣接するセルがこのような上昇流の根の速い動きを強制する。実験結果によると、このプロセスに3つのパターンがある。第1のパターンでは、一つの短寿命のセルからのアウトフローによって上昇流の根が移動する。第2のパターンでは、次々に形成する短寿命のセルのアウトフローの先端に沿って移動する。第3のパターンでは、既存のLタイプセルからのアウトフローとともに移動する。これらのプロセスを経ていったん鉛直シアー風上側に傾いた上昇流がつくられると、セルは地上付近に強い冷気プールを形成して自己維持する。

[1]現在所属：防災科学技術研究所
[2]現在所属：スロバニア水文気象研究所
[3]現在所属：富士通株式会社